Available online at www.sciencedirect.com

SciVerse ScienceDirect

Journal of the European Ceramic Society 32 (2012) 1261–1268

www.elsevier.com/locate/jeurceramsoc

Relation between change of porosity and parameters of grains during annealing of the superconducting ceramics $YBa_2Cu_3O_{7-x}$

M.F. Imayev [a,c], D.B. Kabirova [a,*], R.I. Sagitov [b], Kh.A. Churbaeva [b]

[a] *Institute for Metals Superplasticity Problems, Russian Academy of Sciences, Khalturina str. 39, Ufa 450001, Russia*
[b] *Ufa State Aviation Technical University, K. Marx str. 12, Ufa, Russia*

Received 13 May 2011; received in revised form 17 October 2011; accepted 29 October 2011
Available online 23 December 2011

Abstract

The correlation between changes of porosity and the parameters of grains was studied during the annealing of fine-grained ceramics Y123 with various amounts of phase Y211 in the temperature range 900–990 °C with the aim of revealing the mechanism of pore healing. Y123 grains retain their lamellar shape within the temperature range of annealing. Authenticated cases of growth of grains towards pores via local bulging of a plane surface have not been revealed. Healing of pores is observed only in the temperature range 900–975 °C. The most complete pore healing takes place when secondary recrystallization occurs in the sample with the resulting formation of the microstructure possessing wide distributions of grain sizes and grain aspect ratios. 2D simulations have shown that Y123 behaves like a free-flowing body. During the growth of a microstructure with a large variety of grain sizes and aspect ratios, the grains better fit each other, and pores decrease.

Keywords: Oxide superconductors; Grain growth; Grain size; Platelets; Porosity

1. Introduction

Pores are intrinsic element in the microstructure of high-temperature superconducting (HTSC) ceramics. For example, the porosity of $YBa_2Cu_3O_{7-x}$ (Y123) ceramics sintered without pressure is no less than 10–15%, as a rule, and it is rather difficult to reduce it. Moreover, it is very difficult to eliminate the residual porosity which exists in the final stage of sintering in the form of separate pores. This high porosity exerts a negative influence on the properties of ceramics. Firstly, during sintering, the liquid leaks into pores which results in phase heterogeneity. Secondly, pores are stress concentrators and following heat treatment or deformation they often become the sources of cracks. Therefore, to obtain high-quality pieces using plastic deformation it is important to reduce the amount of pores in the initial sintered material.

The liquidus relations in the system $YO_{1.5}$–BaO–CuO_x in the compositional region near the phase Y123,[1,2] sintering behavior and densification of Y123 powder,[3–5] grain growth[6–8] were studied. It was established that during annealing of Y123 ceramics above 900 °C a thin liquid film is formed on the grain boundaries as a result of the following eutectic and peritectic reactions[1]:

$$e1\text{: Y123} + \mathrm{BaCuO_2} + \mathrm{CuO} \rightarrow \mathrm{L}(e_1) + \mathrm{O_2}, \quad 898\,^{\circ}\mathrm{C} \tag{1}$$

$$e2\text{: } \mathrm{BaCuO_2} + \mathrm{CuO} \rightarrow \mathrm{L}(e_2) + \mathrm{O_2}, \quad 902\,^{\circ}\mathrm{C} \tag{2}$$

$$p1\text{: Y123} + \mathrm{CuO} \rightarrow \mathrm{Y_2BaCuO_5} + \mathrm{L}(p_1) + \mathrm{O_2}, \quad 933\,^{\circ}\mathrm{C} \tag{3}$$

$$m1\text{: Y123} \rightarrow \mathrm{Y_2BaCuO_5} + \mathrm{L}(m_1) + \mathrm{O_2}, \quad 1015\,^{\circ}\mathrm{C} \tag{4}$$

Different mechanisms of sintering of Y123 ceramics can operate in different temperature ranges.[5] The initial stage is driven by solid state sintering between 827 and 894 °C (air). Then, in the range 902–920 °C (air) an intermediate-grain growth stage competes with the rearrangement process associated to the

* Corresponding author. Tel.: +7 347 282 37 35; fax: +7 347 282 37 59.
E-mail addresses: marcel@imsp.ru (M.F. Imayev), dilara@imsp.ru (D.B. Kabirova).
[c] Tel.: +7 347 282 37 35.

0955-2219/$ – see front matter © 2011 Elsevier Ltd. All rights reserved.
doi:10.1016/j.jeurceramsoc.2011.10.046

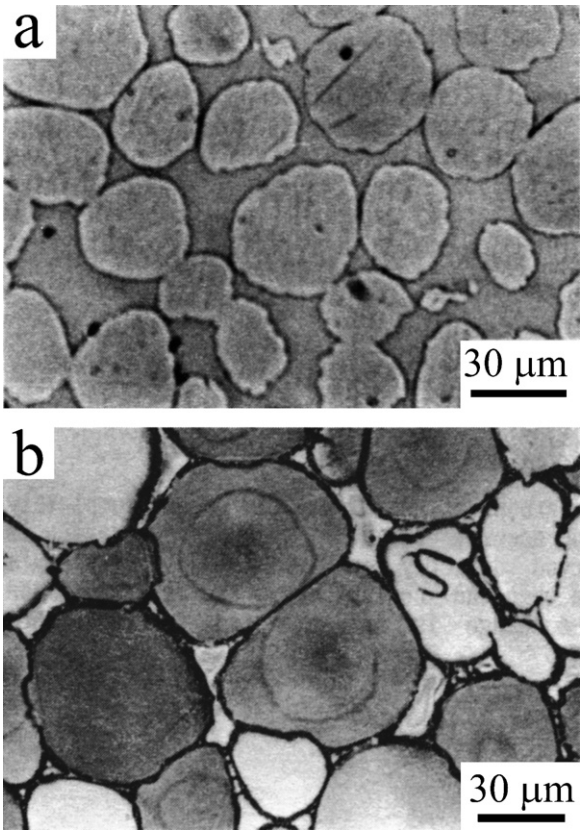

Fig. 1. Microstructure of Mo–15 wt.% Ni alloy sintered at 1450 °C: (a) after short time preliminary sintering in the conditions of large amount of liquid (33 vol.%); (b) after additional sintering with low liquid amount (about 12 vol.%). After preliminary sintering with high liquid content two grains in the center were almost spherical and had a point contact with each other. After reducing the amount of liquid and additional sintering grains have grown primarily in the direction of the pores, therefore the contact surface between these grains grew and became flat and the grains themselves have acquired the form of rounded polyhedrons.[11]

presence of a liquid phase. The next sintering stage in the range 922–970 °C (air) could be fitted by the solution–precipitation model. In the range 972–995 °C (air) the solid state (GG) intermediate stage mechanism and/or viscous flow competes with solution–precipitation process.[5] The operation of such a number of mechanisms should be accompanied by complex grain shape and size changes.

The regularities of the grain size and grain shape evolution which accompany the densification of material during the liquid phase sintering have been studied in detail on refractory W and Mo base alloys, which possess grains of a spherical shape in a state of equilibrium.[9–11] It was found that if the liquid phase is present in a large amount (about 30 vol.%), then the material lightly compacts to a density close to the theoretical. Under these conditions, the solidified liquid occupies the whole intergranular interior and the grains preserve a near-spherical shape (Fig. 1a).[11] When the amount of liquid is small (less than 12%) it cannot fill the intergranular interior completely. In this case the grains themselves fill the pores, causing the change in their shape (Fig. 1b).[11] An important regularity was established, consisting in the fact that the change in the grain shape and reduction

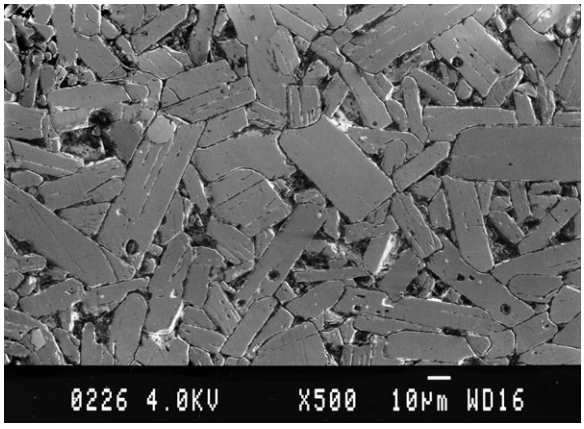

Fig. 2. A typical microstructure of sintered ceramics Y123. Grains keep the lamellar shape near to pores.

in porosity occur mainly due to the directional growth of the grains,[10,11] rather than the preferential dissolution of grains in place of their contact with each other.[9] Grains of the refractory phase grow, come into contact with each other, and then begin to change their shape from spherical to the round polyhedral, tending to grow not in the direction of neighboring grains, but in the direction of the pores (Fig. 1b).[11]

Unlike the refractory W and Mo base alloys the grains of Y123 ceramics have a lamellar shape in the temperature range of liquid phase sintering (above 900 °C), and the lamellar shape is stable up to the incongruent melting point *m1*. Local bulging of lamellas indicating the filling of the pores by grains is not observed near the pores (Fig. 2). The stability of the lamellar grain shape is connected with the low energy of plane surfaces.[12] We did not find in the literature any data dealing with the process of pore healing in materials with a lamellar type structure. In this connection, the healing of pores occurring in HTSC ceramics in the final stage of sintering requires more thorough study. In particular ought to be studied whether any sort of mechanism of grain shape accommodation is active, analogous to that found in materials with equiaxed microstructure.

As shown in Refs. [10,11], grain shape accommodation during the filling process of pores in refractory materials, takes place when rapid grain growth is being realized. For this reason, one can assume that in order to reveal the microstructure changes which accompany a decrease in porosity in Y123, one should initiate rapid grain growth. As a rule, the rapid growth of grains is accompanied by secondary recrystallization, which can be realized efficiently in a fine grained, two-phase composite with a non-uniform distribution of second phase particles.[13] In the case of Y123 such a composite can be produced by introducing Y_2BaCuO_5 (Y211) phase particles.

As shown earlier,[14] the Y123/Y211 composites with different amounts of Y211 and high porosity can be processed by a rather simple method—isothermal annealing of Y123 near the point *m1*. An important peculiarity of such composites is a small amount of liquid phase attributed to the outflow of a large amount of liquid from the sample, resulting from both the low viscosity of liquid and its extrusion by liberated oxygen. As mentioned above, the small liquid amount is a necessary condition for

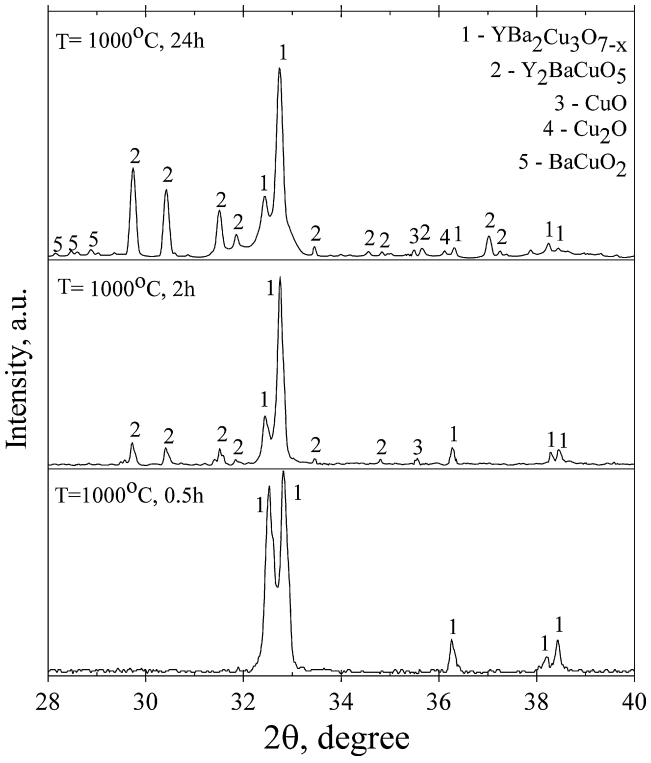

Fig. 3. XRD patterns of the Y123 samples after annealing at 1000 °C for 0.5 h, 2 h and 24 h.

displaying the effect of grain shape accommodation during material densification.[10,11]

The goal of the present research is to investigate the interrelation between changes in porosity and grain parameters during the annealing of fine-grained composites Y123/Y211, with the aim of revealing the mechanism of pore healing in ceramics Y123.

2. Experimental

A rod of fine-grained ceramics Y123, about 30 mm in length, processed by extrusion at 875 °C from Ø10 mm to 5 mm, was cut into 3 portions. The microstructure of ceramics Y123 after extrusion was described in detail in Ref. [15]. For processing composites Y123/Y211 with different amounts of Y211 phase the samples were air annealed at the temperature 1000 °C for 0.5, 2 and 24 h. The processing procedure is described more thoroughly in Ref. [14]. As a result three samples with differing amounts of Y211 phase and pores were produced. The absence of CuO, Cu_2O, $BaCuO_2$ peaks, as well as the decrease in the weight of samples proportionally to the time of annealing, testify that the essential amount of liquid has flowed out from the samples (Table 1 and Fig. 3).

For the study of the interrelation between porosity and the parameters of Y123 grains, the processed samples were subjected to a sequential isothermal annealing for 5 h at the temperatures of 900, 925, 950, 975 and 990 °C and were then air quenched after each annealing. After each "annealing + quenching", microstructure was photographed and

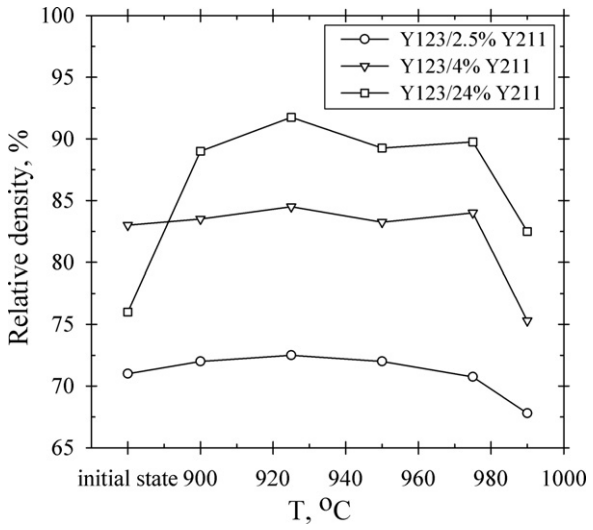

Fig. 4. Dependence of relative density of samples of Y123/Y211 composite on last temperature of sequential annealing. Theoretical density Y123 = 6.36 g/cm^3 and Y211 = 6.22/cm^3.

porosity was measured using the geometric method. The application of the sequential isothermal annealing allows for the studying of microstructural evolution in one and same sample. The study of the microstructure was made using scanning electron microscope JEOL JSM-840. Samples were polished with diamond pastes of various granularity and etched using a 5% solution of perchloric acid in butylalcohol at a voltage of 0.1 V. Parameters of individual grains, namely, their length (l_i), thickness (h_i) and aspect ratio ($a_i = l_i/h_i$), were measured. The number of grains (i) taken into account in each state was 300 and the error of measurement was less than 5%.[16] The volume fraction of phase Y211 was determined by the Glagolev's point count method. The X-ray structural analysis was made on a diffractometer DRON-3M in Cu Kα radiation. The thermal behavior of the batch was studied by DTA on "Derivatograph-C".

3. Results

Two peaks are observed on the DTA curve of the as-extruded sample: at 929 °C (peak *p1*) and at 1015 °C (peak *m1*). The absence of peak *e1*/*e2* on the DTA curve at temperatures of about 900 °C can be explained by low amount of residual $BaCuO_2$ phase in our samples.

Fig. 4 shows the dependence of the density of samples 1–3 on the last temperature of sequential annealing. It is seen that with an increasing annealing temperature the behavior of density is rather complicated. Nevertheless, one can identify a few common features. The density of samples 1 and 3 changes little up to 975 °C (i.e. during four steps of sequential annealing: 900 °C + 925 °C + 950 °C + 975 °C), and then decreases. The most essential changes in density are observed in sample 2. If in the initial state the density of sample 2 is 76% of theoretical, then at 925 °C (i.e. after two steps: 900 °C + 925 °C) it attains 92%. With the temperature of sequential annealing increasing

Table 1
The weight change, quantity of phase Y211 and relative density of the samples annealed at $T = 1000\,^{\circ}C$.

Sample no.	Duration of annealing at 1000 °C, h	Weight change, P/P_o	The quantity of phase Y211, vol.%	Relative density, %
1	0.5	0.96	2.5	83
2	2	0.87	4	76
3	24	0.51	24	71

up to 975 °C the density decreases slightly but it is still high. Above 975 °C the density of sample 2 likewise decreases.

Microstructure and its quantitative characteristics are shown in Figs. 5 and 6, respectively. A lamellar type structure is preserved throughout all annealing steps and there are no distortions of lamellae in the direction towards pores. The change in the mean lamellar thickness is approximately the same in all the cases. With the sequential annealing temperature increasing the rate of increase in thickness is almost the same in all samples (Fig. 6b). The behavior of the lamellar length of samples 1 and 3 is also similar—when the temperature of sequential annealing is increasing it grows steadily (Fig. 6a). However, the behavior of the length of grains in sample 2 is abnormal: up to 925 °C the value of L grows rapidly, but above this its growth is sharply slowed down. The abnormal change in L leads to the abnormal change in the mean aspect ratio of grains A in sample 2. Parameter A achieves its maximum at 925 °C and then decreases slowly. Maximum values of A are observed in samples 1 and 3 at 900 °C and 925 °C, respectively, but they are much weaker than in sample 2 (Fig. 6c). The abnormal growth of A in sample 2 is accompanied by the essential widening of grain aspect ratio distribution, particularly at 900 °C, the value of the standard deviation $\sigma\{a\}$ in sample 2 is much higher than in other samples (Fig. 6d).

The mean grain area ($S = L \times H$)) behaves according to the following: at all temperatures of sequential annealing, the largest grain area is observed in sample 3. In sample 2, the main grain area is close to the ones of sample 3, only at $T = 925\,^{\circ}C$ and 950 °C (Fig. 6e). Nevertheless, the grain area distribution in sample 2 is wider than in other samples. Within the temperature range of 925–975 °C, the standard deviation $\sigma\{s\}$ in sample 2 is twice higher than in samples 1 and 3 (Fig. 6f).

4. Discussion

Sample 2, which is characterized by an essential densification and an abnormal growth of L and such parameters as A, $\sigma\{a\}$ and $\sigma\{s\}$, is of special interest. The abnormal behavior of L and the widening of the corresponding distributions indicate that secondary recrystallization took place in the sample. One should note that it is a typical manifestation of secondary recrystallization in materials with lamellar microstructures. Secondary recrystallization is accompanied by the growth of abnormally coarse lamellae, whereas the fine-grained matrix grows normally. Such a behavior was observed in a number of ceramics.[17–19]

It is obvious that densification in ceramics should be attributed to occurrence of secondary recrystallization. Since the grains of Y123 ceramics, unlike refractory alloys,[10,11] do not change their shape, the densification of sample 2 consequently can be explained by occurrence of a wider grain size and grain aspect ratio distributions (as compared to the other samples)

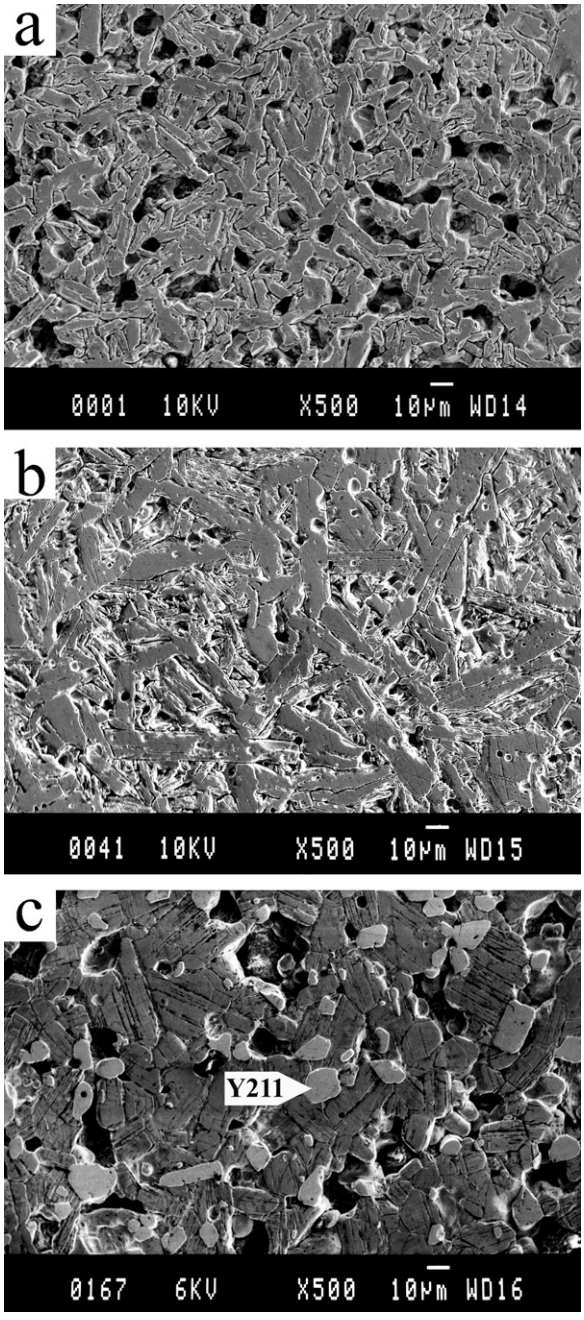

Fig. 5. SEM micrographs of the samples annealed at 900 °C for 5 h: (a) Y123/2.5% Y211, (b) Y123/4% Y211 and (c) Y123/24% Y211.

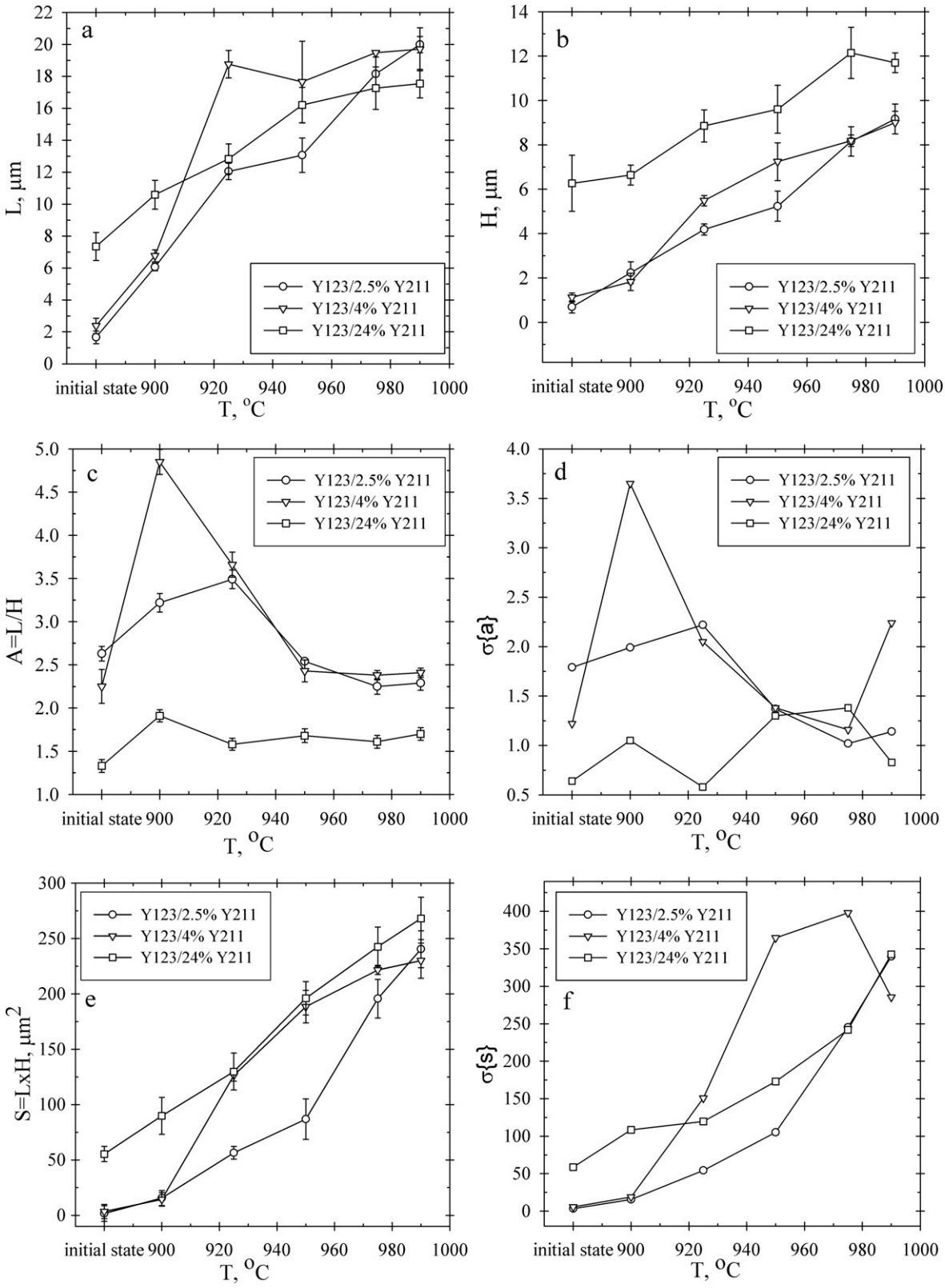

Fig. 6. Dependence of parameters of grains of phase Y123 in composites Y123/Y211 on last temperature of sequential annealing: (a) mean length L; (b) mean thickness H; (c) mean aspect ratio A; (d) standard deviation of aspect ratio $\sigma\{a\}$; (e) mean area S; (f) standard deviation of area $\sigma\{s\}$.

in the process of secondary recrystallization. The behavior of ceramics Y123 is similar to that of a free flowing body, and the process of pore healing has a topological origin. Possessing the largest variety in grain size and grain aspect ratio observed, the densification of sample 2 is denser than that occurring in the other samples, where the variety in these parameters of lamellae is not so essential. However, to prove this assumption we should model the grain stacking. The reason is that at the secondary recrystallization the behavior of a number of parameters, such as A, $\sigma\{a\}$ and $\sigma\{s\}$, is abnormal. A priori it is difficult to identify the parameter in which changes will lead to densification in ceramics.

At the present moment, the stacking of circles and balls has been studied quite thoroughly.[20] It has been established that the degree of stacking in the interior is higher when there are present circles/balls of various dimensions, since small circles/balls tend to fill the spaces between larger ones. The ratio of diameters and the relative number of circles/balls providing maximum stacking density have been calculated.[20] Unfortunately, it is impossible to use the results of circles/balls modeling for describing grain stacking in ceramics Y123 since its grains, being of a disk shape, differ not only in their diameter, but also in the diameter–thickness ratio. We did not find either the papers dealing with 3D modeling of disk stacking or the ones devoted to the 2D modeling of rectangle stacking. In this connection we have made our own modeling.

4.1. Modeling of rectangle stacking

2D modeling was performed. Real grains were replaced by rectangles with narrow and wide distributions of area and aspect ratio. The set of rectangles is processed by a special software—packer GenAlgNor.[21] The program stacks rectangles as densely as possible on the basis of the "pattern cutting–stacking" principle. The sides of the rectangles are parallel to the sides of the stripe, i.e. a rectangle can be stacked parallel to the stripe side or with a 90° turn (see Appendix A). Modeling was performed to reveal the influence of three factors on the density of stacking. These factors are the following: mean aspect ratio of the rectangles A, width of aspect ratio distribution of rectangles $\sigma\{a\}$ (at constant mean area of rectangles) and width of rectangle area distribution $\sigma\{s\}$ (at constant mean aspect ratio of rectangles).

Fig. 7 shows the dependence of stacking density (k) on mean rectangle aspect ratio (A). The mean area of rectangles in each set $S = 1000$ arbitrary units (a.u.). Aspect ratio variation in the set is absent ($\sigma\{a\} = 0$), i.e. rectangles of a strictly definite aspect ratio are selected. The influence on the density of narrow ($\sigma\{s\} \sim 300$) and wide ($\sigma\{s\} \sim 1000$) distribution areas of rectangles is considered. It is seen that with increasing A the density of stacking reduces. The sets with wide area distribution ($\sigma\{s\} \sim 1000$) are characterized by a denser stacking than the sets with narrow distribution ($\sigma\{s\} \sim 300$). The width of aspect ratio distribution also exerts an effect on the density of stacking (Fig. 8). With increasing $\sigma\{a\}$ the density of stacking rises. The sets with wide distribution ($\sigma\{s\} \sim 1000$) give a more dense stacking than the ones with narrow distribution ($\sigma\{s\} \sim 300$).

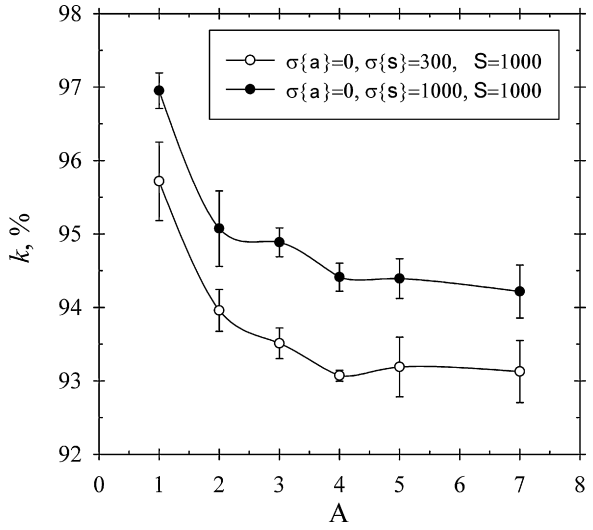

Fig. 7. Dependence of stacking density k on mean aspect ratio of rectangles A.

Thus the results of modeling rectangle stacking have shown the following: under otherwise equal conditions the growth of the mean aspect ratio A is accompanied by a decrease in the density of stacking. This result is evident since more anisotropic rectangles should be stacked less densely. On the other hand, the increase in the variety of size and aspect ratio of the rectangles contributes to an increase in the stacking density because it makes it easier for them to fit with one another.

4.2. Reasons for changes in the density of ceramics Y123

In spite of the fact that the model applied is very simplified and far from a real microstructure, it provides an understanding of general topological regularities and how complex shape particles fill space. Modeling showed that it was an increase in $\sigma\{a\}$, and not in A that led to the growth in density.

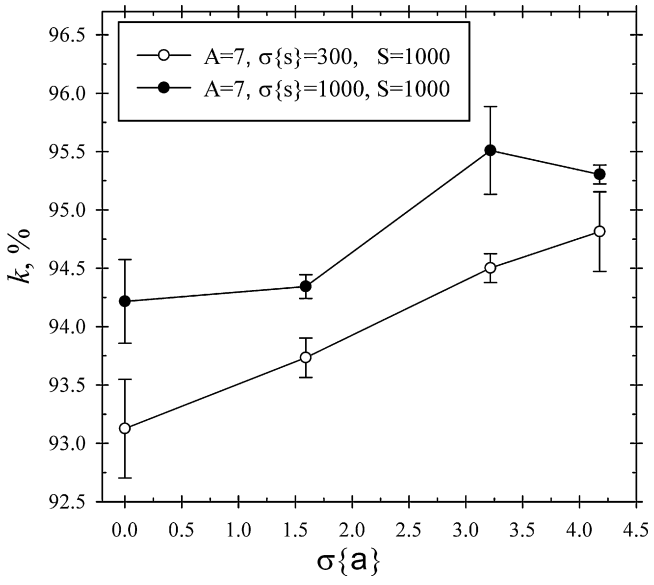

Fig. 8. Dependence of stacking density k on standard deviation of aspect ratio of rectangles $\sigma\{a\}$.

On the basis of the results of the modeling one can assume the following mechanism of pore healing in ceramics Y123. The growth of grains occurs during heating in all states. The growth of Y123 grains is evidently controlled by the Ostwald ripening of particles Y211 and pores. The grain growth is accompanied by continuous topological changes. Due to the disappearance of some grains and the growth of others, the former non-adjacent grains come into contact. Evidently, the current level of porosity directly depends on the size and shape of the grains encountered. In samples 1 and 2, the grain growth occurs normally and distributions of grain sizes and aspect ratios are narrow. In sample 2 (due to a relatively small amount of Y211) a secondary recrystallization takes place which results in a significant variety in size and aspect ratio of the grains. The growth of grains with wide size and aspect ratio distributions leads to a denser filling of the space of a polycrystal than in the samples with narrow distributions of these parameters. In other words, the greater the variety of aspect ratio and size among the grains, the higher the density of the material.

While annealing above 975 °C one can observe an increase in porosity in all samples, including sample 2 where secondary recrystallization took place. This can be explained by the following; firstly, while point *m1* is being approached, the amount of liquid in the sample rises, its viscosity is reduced and its outflow on a substrate becomes more intense. Secondly, since peritectic melting of Y123 is accompanied by the generation of both liquid and oxygen, the latter also contributes to the increase in porosity. At high temperatures the process of loosening in the sample, connected with the release of liquid and oxygen, dominates the process of pore healing initiated by secondary recrystallization. As a result, porosity increases.

5. Conclusion

(1) Grains in ceramics Y123 retain their lamellar shape within the temperature range of annealing (900–990 °C). Reliable data confirming a growth of grains towards pores via local bulging of the plane surface have not been obtained.
(2) Healing of pores occurs only at annealing within the temperature range 900–975 °C. Healing is most intense in the presence of secondary recrystallization which initiates the formation of a microstructure with wide distributions of grain size and grain aspect ratio.
(3) Correlation of density with width of grain size and grain aspect ratio distributions testifies that behavior of ceramics Y123 resembles a free flowing body. When the processed microstructure is characterized by essential grain size and grain aspect ratio variety, the grains fit each other better and the number and size of pores decreases.
(4) At annealing above 975 °C, the porosity practically does not depend on grain parameters and increases in all samples; this is attributed to the large amount of liquid and oxygen generated. Within this temperature range the process of loosening in the sample, connected with the generation of liquid and oxygen, dominates the process of pore healing initiated by the secondary recrystallization.

Appendix A. Modeling of rectangle stacking

The interrelation between grain parameters and porosity in ceramics Y123 has been modeled using a technique of rectangle stacking using the "pattern cutting–stacking" (PCS) algorithm.[22] The essence of this method consists in stacking the rectangles as densely as possible. The semi-infinite stripe of the specified width W is considered. While arranging n various rectangles of specified dimensions (l_i, h_i), $i = 1, \ldots, n$ in this stripe, the following three conditions should be fulfilled: (1) sides of rectangles should be parallel to the corresponding sides of the stripe; (2) rectangles are not to intersect with each other or with the sides of the stripe; (3) the length of the stripe occupied by rectangles should be minimal. The desired optimum of stacking is determined by the rearrangement of the selected array of rectangles. The stacking of elements is completed automatically after attaining a steady minimum level of stripe filling (the largest stacking density of the microstructure model). For convenience when comparing various arrays of rectangles $n = 1000$ was selected. The number of repetitions of stacking was 5.

The size (l_i, h_i) and aspect ratio $a_i = l_i/h_i$ distributions of rectangles were described by a normal distribution. The generation of normal distribution with the specified parameters (mean rectangle dimensions L, H, standard deviations of aspect ratio $\sigma\{a\}$ and area $\sigma\{s\}$, number of rectangles n) was performed using HiMath Computing Package. For stacking the generated set of rectangles the software GenAlgNor developed at the Ufa State Aviation Technical University[21] was applied.

The relative density of stripe stacking with rectangles (k) was calculated by Eq. (A1):

$$k = \frac{S_1}{S_2} \times 100 \tag{A1}$$

where S_1 is the total area of all rectangles and S_2 is the area of the stripe occupied by rectangles.

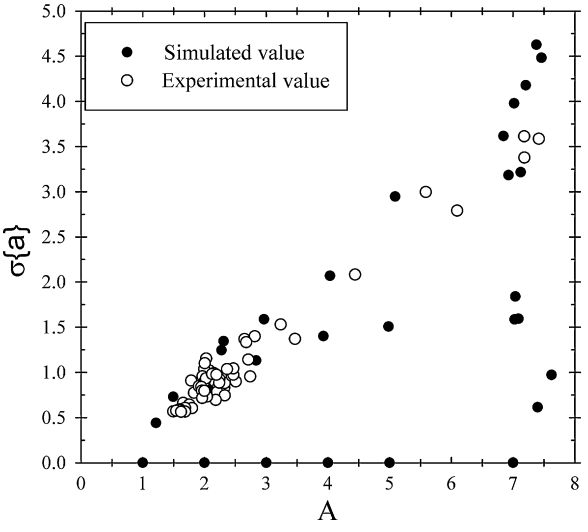

Fig. A1. Combinations $(A; \sigma\{a\})$ of arrays of rectangles used to simulate stacking (full circle). Open circles shows the actual combinations $(A; \sigma\{a\})$ of Y123 grains observed in weakly textured ceramics Y123 after various heat treatments.

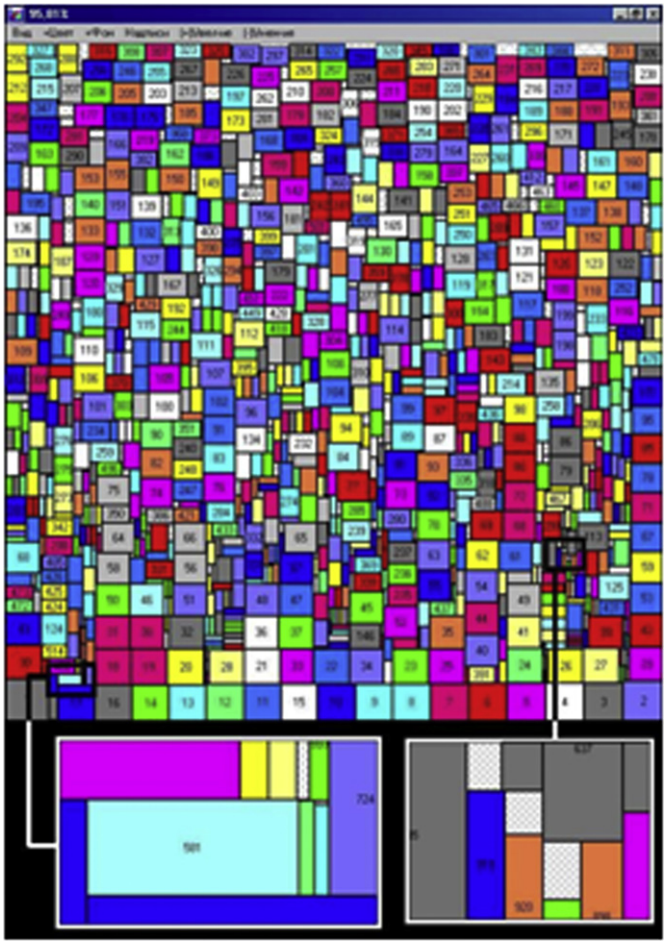

Fig. A2. Example of stacking of rectangles by the program GenAlgNor. Each rectangle is assigned by serial number and color, the pores are shaded. Some fragments of stacking are increased and presented in footnotes. The stacking density is 95.81%.

To equalize the conditions for the arrangement of arrays of rectangles essentially different in size, aspect ratio and width of distribution, a stripe with a shape close to a square was applied. The width of the stripe was calculated by Eq. (A2):

$$W = \sqrt{\sum_{i=1}^{n}(l_i \times h_i)} \tag{A2}$$

Note that it is important to determine ranges of values (A) and corresponding standard deviations $\sigma\{a\}$. We determined this range according to calculations made regarding the real microstructure of ceramics Y123. The non-fill symbols (Fig. A1) indicate real values of A and $\sigma\{a\}$, observed in polycrystal Y123 with a weak crystallographic texture after different thermal treatments. For modeling we used a wider range of values A and $\sigma\{a\}$ (fill symbols). Fig. A2 shows an example of the stacking of a stripe by rectangles.

References

1. Aselage T, Keefer K. Liquidus relations in Y–Ba–Cu oxides. *J Mater Res* 1988;**3**:1279–91.
2. Ullman JE, McCallum RW, Verhoeven JD. Effect of atmosphere and rare earth on liquidus relations in RE–Ba–Cu oxides. *J Mater Res* 1989;**4**:752–4.
3. Ling HC. Preparation and densification of superconducting $YBa_2Cu_3O_x$ ceramics. *J Mater Sci* 1990;**25**:3297–308.
4. Pathak LC, Mishra SK, Mukunda PG, Godkhindi MM, Bhattacharya D, Chopra KL. Sintering studies on submicrometre-sized Y–Ba–Cu-oxide powder. *J Mater Sci* 1994;**29**:5455–61.
5. Benavidez ER, González Oliver CJR. Sintering mechanisms in $YBa_2Cu_3O_x$ superconducting ceramics. *J Mater Sci* 2005;**40**:3749–58.
6. Chu CT, Dunn B. Grain growth and the microstructural effects on the properties of $YBa_2Cu_3O_{7-y}$ superconductor. *J Mater Res* 1990;**5**:1819–26.
7. Shin MW, Hare TM, Kingon AI, Koch CC. Grain growth kinetics and microstructure in the high T_c $YBa_2Cu_3O_{7-\delta}$ superconductor. *J Mater Res* 1991;**6**:2026–34.
8. Imayev MF, Kazakova DB, Gavro AN, Trukhan AP. Grain growth in a $YBa_2Cu_3O_x$ superconductive ceramics. *Physica C* 2000;**329**:75–87.
9. Kingery WD. Densification during sintering in the presence of a liquid phase. *J Appl Phys* 1959;**30**:301–10.
10. Yoon DN, Huppmann WJ. Grain growth and densification during liquid phase sintering of W–Ni. *Acta Metall* 1979;**27**:693–8.
11. Lee D-D, Kang S-JL, Yoon DN. A direct observation of the grain shape accommodation during liquid phase sintering of Mo–Ni alloy. *Scripta Metall Mater* 1990;**24**:927–30.
12. Nakahara S, Fisanick GJ, Yan MF, van Dover B, Boone RT. Correlation of grain boundary defect structure with boundary orientation in $Ba_2YCu_3O_{7-x}$. *Appl Phys Lett* 1988;**53**:2105–7.
13. Novikov VYu. *Secondary recrystallization*. Moscow: Metallurgiya; 1990 [in Russian].
14. Imayev MF, Kabirova DB, Churbaeva HA, Salishchev GA. The effect of temperature on grain growth in $YBa_2Cu_3O_{7-x}$ superconductive ceramics. In: *The first joint int. conf. on recrystallization and grain growth (Rex&GG 2001)*. Aachen: Institute für Metallkunde und Metallphysik RWTH; 2001. p. 339–44.
15. Imayev MF, Imayev RM, Kaibyshev OA, Musin FF, Yamalova MO. Microstructure and superconductive properties of hot-deformed $YBa_2Cu_3O_x$ ceramics. Part 1. Microstructural consideration. *Supercond Sci Technol* 1994;**7**:701–6.
16. Saltykov SA. *Stereometric metallography*. Moscow: Metallurgiya; 1970 [in Russian].
17. El-Raghy T, Barsoum MW. Processing and mechanical properties of Ti_3SiC_2. I. Reaction path and microstructure evolution. *J Am Ceram Soc* 1999;**82**:2849–54.
18. Kim Y-W, Mitomo M, Hirotsuru H. Grain growth and fracture toughness of fine-grained silicon carbide ceramics. *J Am Ceram Soc* 1995;**78**:3145–8.
19. Kunaver U, Kolar D. Computer simulation of anisotropic grain growth in ceramics. *Acta Mater* 1993;**41**:2255–63.
20. Medvedev NN. *Investigation into the structure of noncrystalline systems by Voronoĭ–Delone method*. Novosibirsk- Izd SO RAN NITs OIGGM; 2000.
21. Il'jasova LA. Packing of containers: development and research of multi-method genetic algorithm. Diploma thesis. Ufa: USATU; 2004 [in Russian].
22. Mukhachiova EA, Zalgaller VA. Linear programming cutting problems. *Int J Softw Eng Knowl Eng (IJSEKE)* 1993;**3**:463–76.